



OPEN

Optimization of simultaneous adsorption of nickel, copper, cadmium and zinc from sulfuric solutions using weakly acidic resins

Somayeh Kolbadinejad & Ahad Ghaemi✉

In this research, the adsorption of nickel (Ni), copper (Cu), cadmium (Cd), and zinc (Zn) from real sulfuric leaching solution with weakly acidic resins has been studied using response surface methodology (RSM). The adsorption process on two weakly acidic resins has been investigated as a function of pH, time, temperature, and resin dosage. The experimental results indicate that the amino phosphoric acid resin removed Ni, Cu, Cd, and Zn from an acidic solution very efficiently. Based on the central composite design (CCD) on the RSM, the statistical criteria of correlation coefficient (R^2) values of Ni, Cu, Cd, and Zn are 0.9418, 0.9753, 0.9657, and 0.9189, respectively. The adsorption process followed the pseudo-second-order kinetic model and the thermodynamic calculations indicated the chemical interaction between the resin surface and the metal ions. Enthalpy values greater than zero indicate that the adsorption reaction of the metals is endothermic. The optimal adsorption process was carried out at time of 20 min, temperature of 30 °C, pH of 5, and resin dosage of 4 g/L. In these conditions, the adsorption capacity of nickel, copper, cadmium, and zinc were obtained 13.408, 7.087, 4.357, and 15.040 mg/g, respectively.

Keywords Metal ion, Resin, Adsorption, Kinetic, Thermodynamic, Response surface methodology

Increasing the request of valuable metals such as Ni, Cu, Cd and Zn in various industries and decreasing the primary sources of these metals in nature are the reason for recovering these metals from industrial waste¹. Ni is a hard and corrosion-resistant metal and is used in catalyst production, battery, electrical industries^{2,3}. Cu, like silver and gold, exists in natural state without combining with elements^{4,5}, and due to its electrical conductivity, high workability, and corrosion resistance is used in electronics, military, shipbuilding, construction, and industrial equipment⁶. Cd is harmless to human health up to 0.53 mg/kg, but more than this amount, Cd is a heavy and toxic metal^{7,8} that from melting and extracting metals enters to the environment⁹. Zn, despite being useful for human health, causes poisoning in excess of the permissible limit¹⁰. The filter cakes of the Zn industry contain Ni, Cu, Cd, Zn and etc. which can be considered as a secondary source for the supply of these metals, therefore, the recovery of precious metals is needed and includes leaching and separation steps^{11,12}. In the leaching stage, there are heterogeneous reactions between the solid phase and the liquid phase and the solid phase is dissolved¹³, but dissolution is not selective and requires the selective separation of desired metals in the next steps^{14,15}. The recovery of metal ions from the leaching solution depends on the pH, composition, concentration of ions in the solution. Among processes, it can mention sedimentation¹⁶, electrowinning¹⁷, solvent extraction¹⁸ and ion exchange resin¹⁹. In order to reduce industrial costs, resins are used for some reasons such as: in the reversible process of using cationic/anionic resins, the ion exchange between the cation/anion in the functional group of the resin occurs with the cation/anion in the solution, respectively. Equation (1) shows the ion exchange reaction for cationic resins^{20,21}:



Functional groups give properties such as acid, alkali or chelation to resins. There are four main types: strong acid, strong alkali, weak acid and weak alkali, whose functional groups are different²². Fixed bed columns are used for industrial applications²⁰ and adsorption selectivity is related to the metal complex at any pH^{22,23}. Sufficient residence time is one of the important factors to increase adsorption efficiency. If the flow intensity increases,

School of Chemical, Petroleum and Gas Engineering, Iran University of Science and Technology, Tehran, Iran. ✉email: aghaemi@iust.ac.ir

adsorption efficiency decreases due to the reduction of required time²⁴. Adsorbents are classified into: carbonaceous materials, industrial and agricultural wastes, polymer adsorbents, mineral materials, bio adsorbents, composites and adsorbents with special structure²⁵.

Based on the studies, some resins such as: amberlite IRC 748²³, Pyrolite S 930^{26,27}, Lewatit Mono-Plus TP 207 XL²⁸, NDC 984²⁹, activated carbon prepared from sewage sludge³⁰ nano graphite³¹ and various nanocomposites³² are more selective to the separation of Ni from Cd, Cu and another metal ions. Results of comparisons between Amberlite IRC 748, Unac SR 5, Prolite S 930 and Dowex M 4195 resins for adsorption of Ni and Co from high pressure acid leaching solution, show more nickel is adsorbed by Dowex M 4195 than the other resins³³. NPG@Fe₃O₄ nano-adsorbent was produced with mixing of graphene nanoparticles and Fe₂O₃ and Fe₃O₄, which allows easier separation of Ni from aqueous solutions³⁴. D 401 chelate resin²⁴, S930 chelate resin^{27,35}, resin derived from acrylonitrile-divinylbenzene copolymers³⁶, Dowex M4195^{37,38}, Levatite TP 220^{38,39} and WRAM¹⁵, polyglycidyl methacrylate-glycine porous chelating resin⁴⁰, resin with group of polyhydroxamic acid—polyamidoxime⁴¹, chelating group of amidoxime⁴², Dowex XUS 43578⁴³, cross-linked magnetic chitosan⁴⁴, Magnetite Nano-Adsorbent (MNA)⁴⁵, magnetic chitosan beads (MCSB)⁴⁶, sawdust chitosan nanocomposite beads⁴⁷, melamine-diethylene triamine pentaacetic acid resin⁴⁸, nanocomposite powder activated with biological materials⁴⁷, granular activated carbon produced from palm kernel shell⁴⁹, coal fly ash⁵⁰, bio adsorbent⁵¹, activated carbon prepared from sugarcane papyrus⁵², Zeolite-Based Geopolymer adsorbents⁵³, a novel nanocomposite adsorbent, graphene oxide modified with magnetite nanoparticles and Lauric acid containing ethylenediaminetetraacetic acid (GFLE)⁵⁴, Hydroxy propyl picolyl amine (HPPA)⁵⁵ are useful for selective recovery of Cu, Zn and Cd. The several resins including Dowex M 4195 (bis-picolylamine), Amberlite IRC 748, Prolite S 930 (iminodiacetate) and Prolite S 991 (amine/carboxylic) are more selective for Cu in the solution containing Ni, cobalt, iron, Zn, manganese and aluminium⁵⁶. Adsorption of Cu in acidic streams was studied using polymeric resins including Levatite Monoplas TP220, Levatite Monoplas SR7, Levatite AF5, Prolite A 830, Prolite S 984, Prolite A 40 TL and Dox PSR 2. The adsorption efficiency of Cu was the highest using TP220 Monoplas Lavatite⁵⁷. The adsorption behavior of Lewatit MonoPlus TP220 for Cu in the presence of ABSNa50 surfactant was better than other adsorbents (adsorption capacity ≈ 10 mg/g)⁵⁸. Polymeric adsorbent of Amberlite XAD7HP used for As, Cd and Pb metallic ions recovery⁵⁹. A new chelating resin with chemical modification of styrene-divinylbenzene copolymer adsorbed toxic metal ions from aqueous environments⁶⁰. The adsorption of Cd, Ni, Cu and Pb from the aqueous solution has occurred with amberlite IRA 402 and amberlite XAD7HP that were functionalized by chelating agent Direct red 23 (DR 23). The adsorption of Cd was higher than other ions⁶¹. A summary of the operating conditions and functional groups of the industrial resins is given in Table 1.

Polymeric resins have advantages such as non-volatile, chemical stability, insoluble in water and can be reused in subsequent surface adsorption cycles. A "weak" acidic resin will only ionize within a limited pH range. While a "strong" acidic resin shows no change in ion exchange capacity with pH changes. The ion exchange capacity of weakly acidic resin depends on pH value of solution. Also, weakly acidic resins can gain or lose protons with buffer pH changes. Regeneration and recharge provide another feature of selectivity for these types of resins.

Nowadays, response surface methodology (RSM) is one of modeling and optimization method that is used for understanding the behavior of systems in chemical processes and optimizing their performance^{62,63}. RSM reduces systematic errors by estimation of investigational error and also requires fewer computer simulations with fewer experiments⁶⁴.

It is noted that the recovery of heavy metals as a secondary resource is still an evolving research area and there is scope for optimization and integration of new and/or existing technologies.

Resin type	Functional groups	Operating conditions				Reference
		Time (h)	Temperature (°C)	pH	S/L (g/l)	
Amberlite IRC 748	-CH ₂ N-(CH ₂ COOH) ₂	-	25	5	2.5	23
Pyrolite S 930	-N(CH ₂ COOH) ₂	6	20	2.5	1:10	26
Lewatit Mono-Plus TP 207 XL	NH(OOH) ₂	24	25	-	-	28
Activated carbon prepared from sewage sludge	Carbon-Based materials	1.5	55	8	4	30
Nano Particles of Graphon (NPG)@Fe ₃ O ₄	Carbon-Based materials	0.5	25	9	-	34
Dowex M4195	Bis(2-pyridylmethyl) amine	3.5	50	-	-	37
Magnetite Nano Adsorbents (MNA)	Magnetic-Based materials	-	25	5.4	0.05	45
Glutaraldehyde Cross-Linked Magnetic Chitosan	Magnetic-Based materials	6	28	5	1.5	46
Sawdust Chitosan Nanocomposite		1.1	30	5-6	0.05	47
Dealumination of Coal Fly Ash	Coal Fly Ash	6	25	8	-	50
Activated carbon prepared from sugarcane papyrus	Carbon-Based materials	1	25	6	30	52
Zeolite-Based Geopolymer adsorbents	Zeolite-Based materials	2	25	-	2	53
Nano composite adsorbents	Graphene oxide/ Lauric acid + Ethylenediaminetetraacetic acid nanoparticles (GFLE)	1.45	40	1	0.28	54
XUS43605	Hydroxy propyl picolyl amine (HPPA)	2	25	2	-	55
Lewatit Mono-Plus TP 220	Bis(2-pyridylmethyl) amine	24	25	-	-	58

Table 1. Operating conditions and functional groups of the industrial resins.

The innovation of the current research is the optimization of the simultaneous adsorption conditions of metals including Ni, Cu, Zn and Cd from the pregnant leaching solution obtained from the low-grade filter cake. Two weakly acidic resins including CH020 and CH030 have been used for adsorption of the metals from the leaching solution. The RSM model was used for experimental modeling and optimization of the process. The kinetic and thermodynamic adsorption models have been investigated to identify the resins behavior. The effect of operating parameters including temperature, pH, time and the resin dosage on adsorption rate of Ni, Cu, Zn and Cd were evaluated.

Material and methods

Materials

In the experiments, the leach solution was obtained by leaching of low-grade filter cake from Zn factory. The leaching solution was prepared at solid-liquid ratio of 0.09 g/mL, particle size of 177 mic and of pH 1.5. According to the leaching solution, it is tried to separate Ni, Cu, Zn and Cd by surface adsorption with resins by commercial titles of CH020, CH030, C100, and C100E from Canftech Company. The solution pH was preserved by sodium hydroxide for a range between pH 2 to 10. Chemicals like sulfuric acid 98%, distilled water, and sodium chloride have been bought from Merck.

Methods

The RSM based on CCD approach is a set of statistical technique for experimental modelling of the process. Also, RSM was used for optimizing the Ni, Cu, Cd and Zn adsorption affected by several independent variables and reducing the number of experiments⁶⁵⁻⁶⁷. The quadratic polynomial for predicting the optimal effects of effective parameters is expressed in Eq. (2).

$$y = \beta_0 + \sum_{i=1} \beta_i X_i + \sum_{i=1} \beta_{ij} X_i^2 + \sum_{i=1} \sum_{j=i+1} \beta_{ij} X_i X_j + \varepsilon \quad (2)$$

where y is the predicted response, β_0 is the offset term, X_i and X_j are the independent variables, β_{ii} and β_{ij} are the interaction coefficients, respectively. ε is an unpredicted parameter that is determined experimentally. The aqueous samples were analyzed by flame atomic absorption spectroscopy (AAS/ model: WFX-220B) with Eq. (3), the adsorption capacity of resin can be calculated as follow:

$$q_e = \frac{(C_i - C_e)V}{m} \quad (3)$$

where q_e is the adsorption capacity (mg/g), where C_i and C_f are the initial and final ion concentrations, respectively, m is the mass of used resin (g) and V is the solution volume (L^{-1}). The adsorption percentage of each metal ion is determined by Eq. (4):

$$Adsorption (\%) = \frac{C_i - C_f}{C_i} \times 100 \quad (4)$$

The statistical criteria of correlation coefficient (R^2) was used to evaluate the accuracy and performance of the model, and the accuracy between the predicted values and the actual values⁶⁸. R^2 was calculated as follow:

$$R^2 = \sum_{i=1}^n (X_{predicted} - X_{actual})^2 / (X_{predicted} - X_{mean})^2 \quad (5)$$

where X_{actual} and $X_{predicted}$ are the experimental and the predicted values by RSM, respectively. X_{mean} is mean value of data and n is the number of data points.

Temperature, pH, resin dosage and time are independent variables. The combination of two resins was also considered as an effective factor. Alpha is the distance of each point from the center in a centered composite design. Points in the cube represent alpha values less than one, values on the faces of the cube represent alpha equal to one, and points outside the cube represent alpha greater than one. Here, alpha is chosen equal to 2 and the values between the minimum and maximum of each parameter are divided into 5 parts. Design experiment software proposed 60 experiments that their coding and actual values are given in Table 2.

Independent variables	Unit	Coded variable	Coded variable				
			-2 α	-1 α	0	+1 α	+2 α
Time	min	A	5	10	15	20	25
Temperature	C	B	25	30	35	40	45
pH	-	C	2.0	3.0	4.0	5.0	6.0
Resin concentration	mg/10cc	D	20	40	60	80	100

Table 2. Independent numerical variables with the actual and coded levels.

Adsorption experiments

To start the experiments, it is necessary to prepare an acid leaching solution containing Ni, Cu, Cd and Zn ions. The leach solution was obtained by dissolving 13.5 g of low-grade filter cake with size of 177 microns in 150 cc of water and sulfuric acid solution with pH of 2.5 at 40 °C for 1.5 h. In the next step, preliminary tests were performed to determine the range of important and effective parameters using CH020, CH030, C100 and C100E resins. According to the obtained results, two resins: CH020 and CH030 and the parameters of temperature, time and pH, and resin dosage were selected to continue the experiments. Based on the RSM, 60 experiments were performed in different conditions. In this way, 10 ml of leaching solution with a certain pH was placed as a feed in a special container with a 200-rpm stirrer in a water bath to adjust and stabilize the temperature. After reaching the desired temperature, the dosage of resin was added to the solution. After the required time, the sample was separated using filter paper. The initial and final concentrations of Ni, Cu, Zn and Cd in the leaching and adsorption solution were measured by flame atomic absorption spectroscopy (AAS/ model: WFX-220B). After every 60 samples, three standard solutions of metal ion were run to confirm the reliability of the results by the AAS. All experiments were performed in triplicate to determine their reproducibility, and the average concentration was determined using the mean and standard deviation (\pm SD).

The resins scanning electron microscopy-energy dispersive X-ray spectroscopy (SEM, EDX) and X-ray diffraction (XRD) was done to identify physical and chemical properties.

Cantech CH020 and CH030 are a sort of chelating resin which have weakly acidic iminodiacetic acid $[-\text{CH}_2\text{N}-(\text{CH}_2\text{OOH})_2]$ and weakly acidic amino phosphonic $[-\text{CH}_2\text{NCHH}_2\text{PO}_3^-]$, respectively, in the styrene and divinylbenzene (DVB) copolymer with special microporous structure. The crosslinked styrene–divinylbenzene copolymer forms the structure of ion exchange resins. The interaction of CH020 and CH030 functional groups with metal cations are provided in Eqs. (6) and (7), respectively.



Resin regeneration

For regeneration, 10 cc of 20% (w) of sulfuric acid was added to the resin and stirred for 5 min at room temperature with a stirrer at 200 rpm. Then, the final concentration of metal ions in the aqueous phase was measured by flame atomic absorption spectroscopy (AAS/ model: WFX-220B) with acetylene–air flame atomization. The regenerated resin was reused in the adsorption cycle. This cycle was repeated up to 5 times with the same amount of adsorption. The regeneration results showed that the resins can be used several times without loss of absorption capacity.

Results and discussion

Resin characterization

The formed materials and the crystallographic structure had been characterized by X-Ray diffraction analysis (XRD). The higher intensity of the resulting peak shows the higher crystallinity percentage of the sample and the more regular arrangement of the polymer chains. But the more irregular arrangement of the chains indicates by the wider resulting peak. According to Fig. 1a, b, the arrangement of the polymer chains in the two resins is regular and there is more opportunity and possibility of ion exchange.

The scanning electron microscope (SEM) uses a focused beam of high-energy electrons to generate a variety of signals at the surface of solid specimens for analysis of the surface morphology of the resin before and after adsorption. Images of resins CH030 and CH020 by SEM are shown uniform microporous structure on the regular spheres in Fig. 2. Polymer particles have diameters in the range of 550–600 μm . After the ion exchange process, in the surface morphology of resin can be seen a small difference in the form of roughness. These changes are not much due to the structure of the resin, and for this reason, the resin can be regenerated and reused.

Effect of operating condition on adsorption capacity

Adsorption capacity of metal from the liquid phase depends on several physicochemical factors including pH of solution, resin type and dosage, temperature, time, initial metal concentration and presence of other cations. In the experiments, an acid leaching solution of low-grade waste containing various metal ions is used for the metals removal. The effect of time, temperature, pH and resin dosage on adsorption capacity are investigated.

pH is one of the most important and crucial parameters in the adsorption of Ni, Cu, Cd and Zn. Metal precipitation, ionization degree and activity of the resin functional group are considered in the pH adjustment⁷⁶. Changes in the pH level and the presence of hydrogen ions in the solution affect the rate of ion exchange^{77,78}. The experiments were done with 5 g/L of CH030 in the leaching solution at room temperature for 30 min in the pH range of 2–10. According to Fig. 3, the changes in initial pH are very extensive due to the effects of pH on the structure of the resin. At pH between 2 and 4 due to the increase of H^+ and its competition with metal ions for resin sites, electrostatic repulsion occurs with the resin and smaller amounts of adsorption are observed. But at pH range of 4–6, a significant increase in adsorption values is observed due to the reduction of positive ions on the surface of the resin and reached a peak at pH 5–6 and then slightly constant. In pH of 6–10, metal ions can generally be precipitated as a hydroxide in solute^{79,80}. With the increase of pH and increasing of OH^- , metal cations have a greater tendency to form hydroxide deposits and sediments instead of adsorption, and real adsorption studies become impossible with the accumulation of precipitation on the resin surface. To avoid the precipitation of Ni, Cu, Cd and Zn ions, the adsorption process should be carried out at a pH lower than 6.

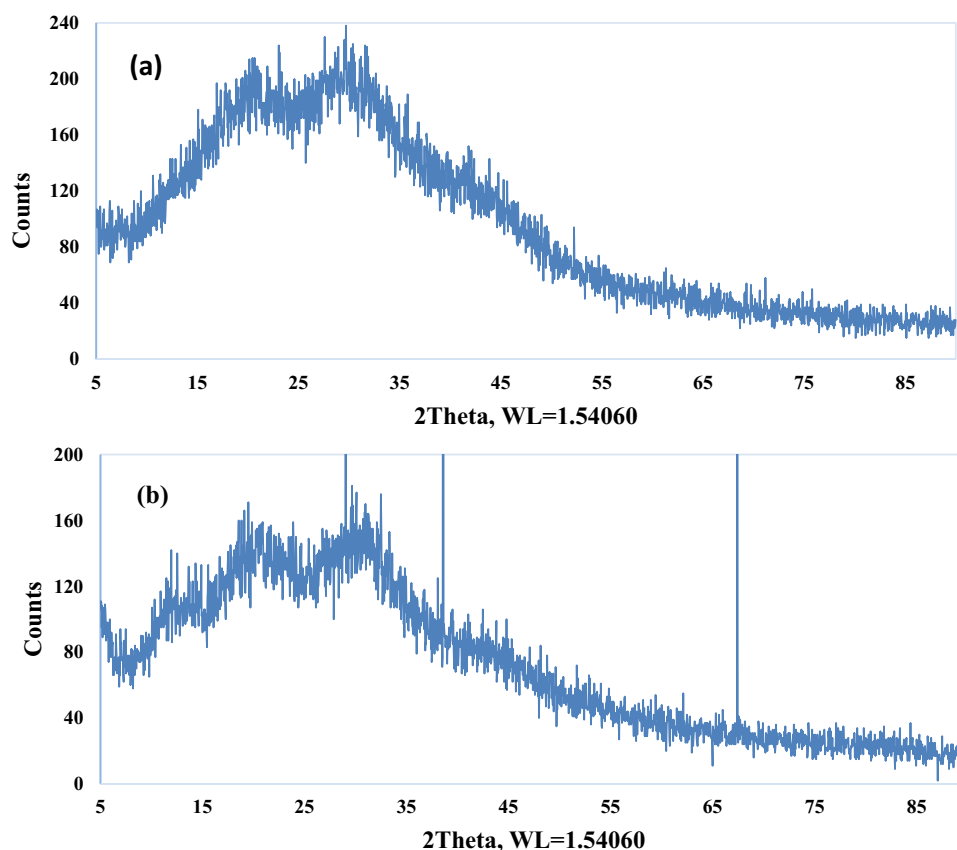


Figure 1. X-Ray diffraction analysis (XRD) of resins (a) CH020 and (b) CH030.

Figure 4 shows the effect of time on the adsorption of Ni, Cu, Cd and Zn. The time to reach the equilibrium of the two phases is an important parameter for maximum adsorption⁸¹. The adsorption of the desired ions with 5 g/L of resin from solution at room temperature was fast in the first 30 min because of large number of free surfaces for adsorption and almost the equilibrium was reached for all desired ions after 30 min.

The adsorption process on CH020, CH030, C100, C100E resins were carried out at 5 g/L of each resin in leaching solution and pH of 4, temperature of 25 C and time of 30 min. CH030 resin has the highest adsorption of Ni, Cu, Cd and Zn ions due to the presence of amino phosphonic functional groups. After selection of resin type, experiments were conducted to determine the resin dosage. According to Fig. 5a, by increasing the dosage of resin from 1 to 5 g/L, the adsorption of the desired metals increases due to the increase of the contact surface⁸². The adsorption capacity increased rapidly from 1 to 3 g/L and remained almost constant from 3 to 5 g/L.

There are many disturbing ions in the adsorption solution, and a part of the active surface of the adsorbent is filled with these disturbing ions, so the adsorption capacity for the desired ions is reduced.

RSM results

According to the general definitions in the software manual, models can be considered acceptable if their p-value is less than 0.05 and the lack of fit value of that model is greater than 0.05. According to the analysis of variance (ANOVA) results, single parameters and interactions of the parameters on the model could be explained. ANOVA also contains the sum of squares, degree of freedom (df), mean square, model significant (F) value, and probability (p) value^{83,84}. The p-value for both results less than 0.05 is significant, and the lack of fit greater than 0.05 is insignificant⁶⁴. Therefore, the analysis of the variance of the quadratic model is approved. R^2 values for of Ni, Cu, Cd and Zn are 0.9418, 0.9753, 0.9657 and 0.9189, respectively. The results show that the experimental values are well-fitted to the predicted values. ANOVA quadratic regression model for Ni and Cu recovery are presented in Table 3.

The quadratic regression model equations for Ni, Cu, Cd and Zn adsorption in terms of coded factors are given below as Eqs. 8–11, respectively. This equation should not be used to determine the relative effect of the parameter because the coefficients are scaled to match the units of each parameter in the center of the design space. Equation (8) shows that pH is the most effective parameter on nickel adsorption, and with increasing of pH, the amount of nickel adsorption also increases. From Eqs. 9–11, it is concluded that the amount of resin is the most effective parameter on the adsorption of copper, cadmium and zinc. Of course, for all three desired ions, the amount of adsorption decreases with increasing amount of resin.

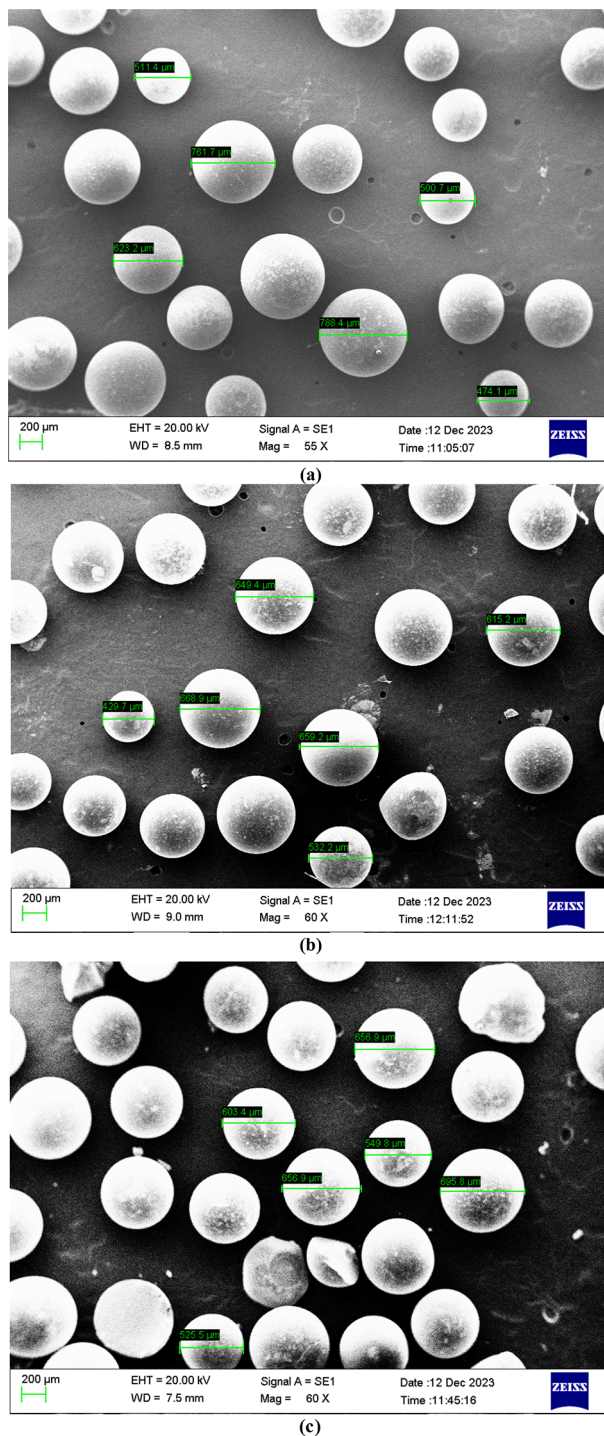


Figure 2. The scanning electron microscope (SEM) of resins before ion exchange: (a) CH020, (b) CH030 and after ion exchange, (c) CH030.

$$\begin{aligned}
 q(\text{Ni}) = & 6.03 + 0.7064A + 0.0124B + 2.35C - 1.71D - 0.0188E - 0.0227AB \\
 & - 0.3237AC - 0.2945AD - 0.1631AE - 0.0341BC + 0.0470BD - 0.0822BE - 1.22CD \\
 & + 0.2748CE + 0.0822DE - 0.3351A^2 + 0.0780B^2 + 1.36C^2 + 0.1371D^2
 \end{aligned} \quad (8)$$

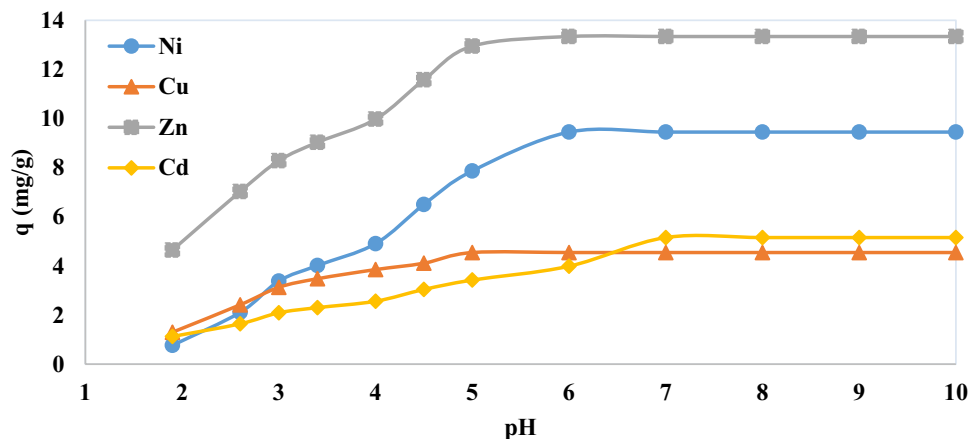


Figure 3. Effect of pH on the adsorption of Ni, Cu, Cd and Zn (mg/g) from aqueous solution by CH030 (time 30 min, room temperature, 5 g/L of resin).

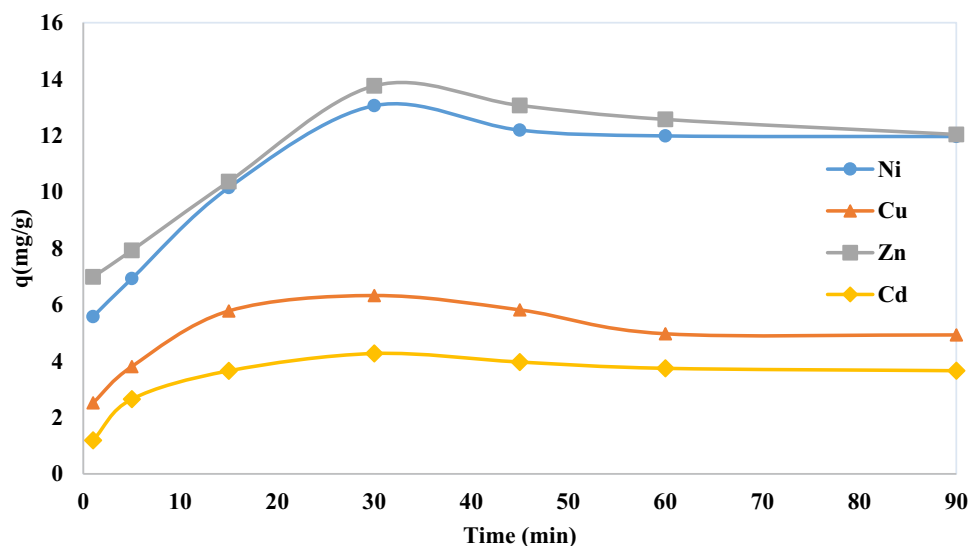


Figure 4. Effect of time on the adsorption of Ni, Cu, Cd and Zn (mg/g) from aqueous solution by CH030 (room temperature, pH 4, 5 g/L of resin).

$$q(\text{Cu}) = 2.83 + 0.1615A + 0.0037B + 0.8300C - 1.39D - 0.0049E - 0.0116AB - 0.1719AC - 0.1705AD - 0.0077AE - 0.0127BC + 0.0017BD - 0.0208BE - 0.3878CD - 0.0171CE - 0.0325DE + 0.0974A^2 + 0.01535B^2 + 0.6171C^2 + 0.5793D^2 \quad (9)$$

$$q(\text{Cd}) = 2.84 + 0.3322A + 0.0169B + 0.3040C - 0.5632D - 0.0173E + 0.0927AB - 0.2393AC - 0.1491AD - 0.1209AE - 0.1336BC + 0.0472BD - 0.0488BE - 0.3219CD + 0.0257CE - 0.2036DE - 0.1153A^2 + 0.0185B^2 + 0.0426C^2 - 0.0338D^2 - 0.1138ABE + 0.0497ACE + 0.0773ADE + 0.1907BCE + 0.0155BDE + 0.0872CDE + 0.0234A^2E - 0.0011C^2E + 0.1041D^2E \quad (10)$$

$$q(\text{Zn}) = 8.44 + 0.8534A + 0.1038B - 0.5268C - 3.24D + 0.4303E - 0.1336AB - 0.4819AC - 0.4685AD - 0.2131AE - 0.0785BC + 0.0753BD - 0.1776BE - 0.3021CD - 0.1658CE - 0.3675DE - 0.1835A^2 + 0.2395B^2 + 0.0923C^2 + 1.81D^2 \quad (11)$$

Based on the results, the regression model obtained from CCD is consistent with the experimental values and is used to optimize the experimental parameters. The conditions of data normality for Ni, Cu, Cd and Zn and the dispersion of data to identify with more errors were recognized for model correction. For model validation, the difference between the actual and predicted data is calculated and defined as the residual⁸⁵. According to Fig. 6,

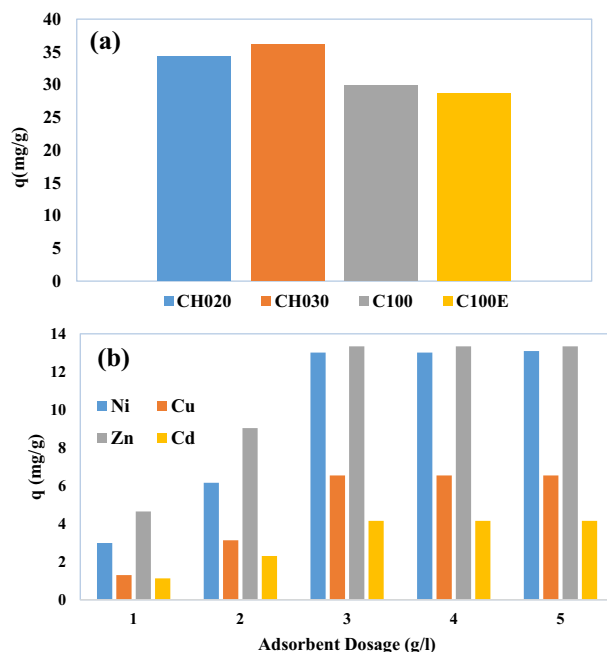


Figure 5. (a) Total adsorption of Ni, Cu, Cd and Zn (mg/g) by 5 g/L of CH020, CH030, C100 and C100E (at time 30 min, temperature of 25 C, pH of 4) and (b) Effect of resin dosage on the adsorption of Ni, Cu, Cd and Zn (mg/g) by CH030.

Source	Sum of Squares	df	Mean Square	F-value	p-value	
Response 1: Ni						
Model	420.17	19	22.11	31.51	<0.0001	Significant
Residual	25.97	37	0.7018			
Lack of Fit	18.67	27	0.6916	0.9479	0.5722	Not significant
Response 2: Cu						
Model	133.44	19	7.02	76.87	<0.0001	Significant
Residual	3.38	37	0.0914			
Lack of Fit	2.06	27	0.0764	0.5796	0.8741	Not significant
Response 3: Cd						
Model	37.33	29	1.29	26.25	<0.0001	Significant
Residual	1.32	27	0.0490			
Lack of Fit	1.06	18	0.0587	1.98	0.1480	Not significant
Response 4: Zn						
Model	470.73	19	24.78	21.47	<0.0001	Significant
Residual	41.54	36	1.15			
Lack of Fit	35.76	26	1.38	2.38	0.0766	Not significant

Table 3. ANOVA quadratic regression model for Ni, Cu, Cd and Zn adsorption.

the results show that the error rate for all responses is normally distributed and the adequacy of the model is confirmed.

Figure 7 shows that the effectiveness of the resin dosage and pH on Ni, Cu, Cd and Zn adsorption⁷⁷. These essential variables in adsorption of desired metals are compatible with the results of the ANOVA model. By increasing the pH, the competition between the H⁺ and the positively charged metal ion at the surface of resin is reduced. Also, with the increase of OH⁻, metal cations have a greater tendency to form complexes and sediments instead of adsorption, and real adsorption studies become impossible with the accumulation of sediment on the resin surface⁸⁶. Based on Fig. 9, increasing the resin dosage has a decreasing effect on the amount of metal adsorption. By increasing the surface area of the resin to the optimum value increases the efficiency of adsorption⁸². But more than optimum point, due to the overlap of the adsorption sites as a result of excessive crowding of the resin particles and also reduction of the contact time required to reach equilibrium, reduces the dosage of adsorption.

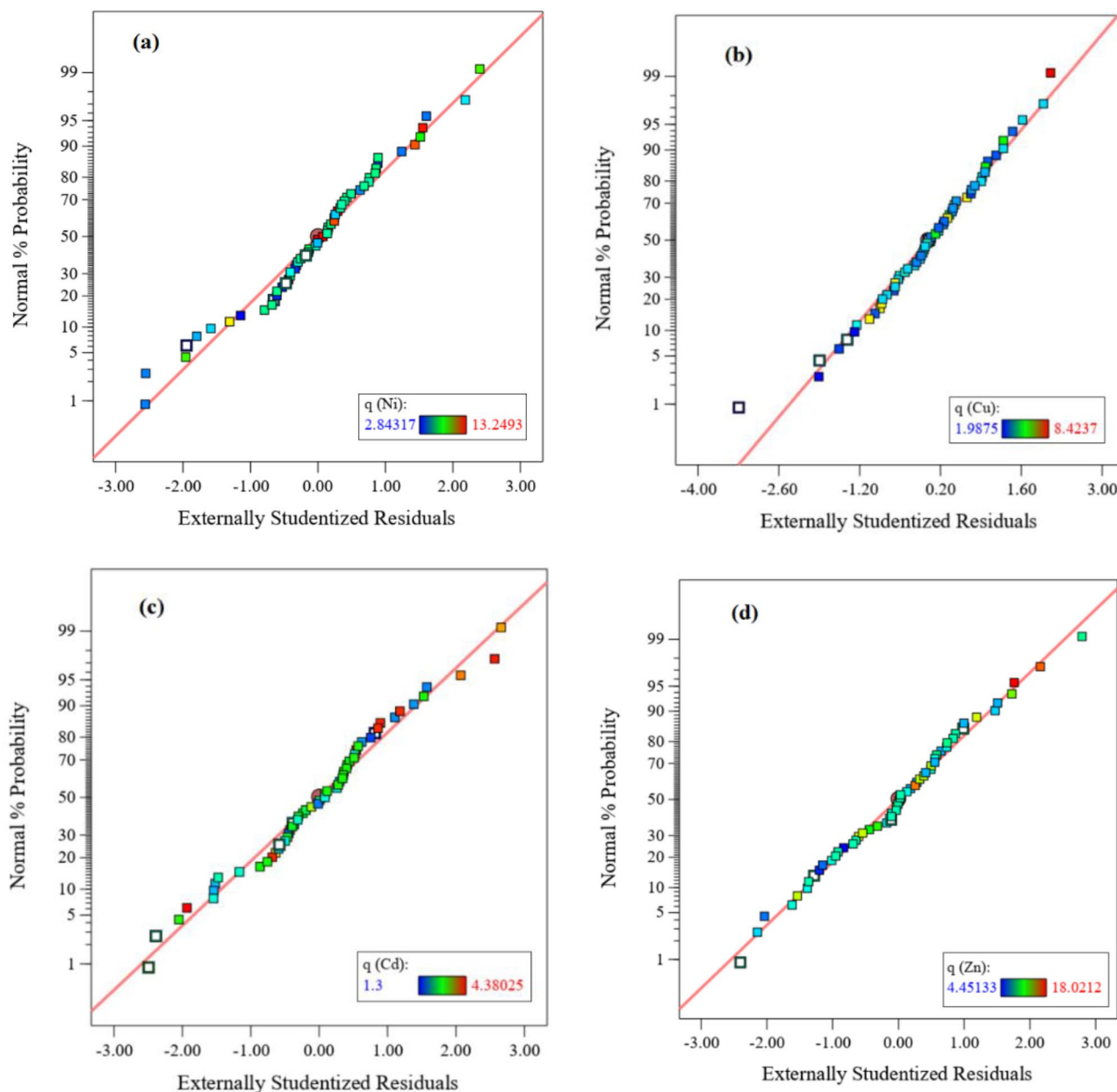


Figure 6. Residual normal probability of (a) Ni, (b) Cu, (c) Cd and (d) Zn.

The optimal adsorption process was carried out at time of 20 min, temperature of 30 °C, pH of 5 and resin dosage of 2 g/L. In these conditions, the adsorption capacity for nickel, copper, cadmium and zinc were obtained 13.408, 7.087, 4.357 and 15.040 mg/g, respectively.

Considering the importance of the simultaneous adsorption of Ni, Cu, Cd and Zn from real leaching solution and evaluation of the interactions of the effective variables in pairs were presented in below. Response surface plots for Ni, Cu, Cd and Zn adsorption versus time and temperature parameters are shown in Fig. 8a–d, respectively. As shown, the highest recovery efficiency is achieved at 30 °C for 20 min. Metal adsorption capacities of the resin increases with increase in adsorption time⁷⁷. The adsorption rate increased sharply in first 20 min because Ni, Cu, Cd and Zn took more chance to be adsorbed by binding sites. Adsorption rate for Ni and Cd decreased than the first 20 min because the majority of resin sites was saturated. But adsorption rate for Cu and Zn after 20 min increases slowly, which these two ions need more time to reach equilibrium conditions. Temperature has not shown much influence upon the adsorption of Ni and Cd. But for Cu and Zn adsorption, the observed decrease in adsorption rate with increasing temperature indicates weak binding interaction between active sites and metal ions, which supports physical adsorption⁸². In addition, physical adsorption reactions are usually exothermic. Hence, the adsorption rate generally increases with decreasing temperature.

The effect of resin dosage and pH on Ni, Cu, Cd and Zn adsorption is shown in Fig. 9a–d, respectively. By increasing the resin dosage more than 2 g/L and probably overlapping of particles, the contact surface decreases.

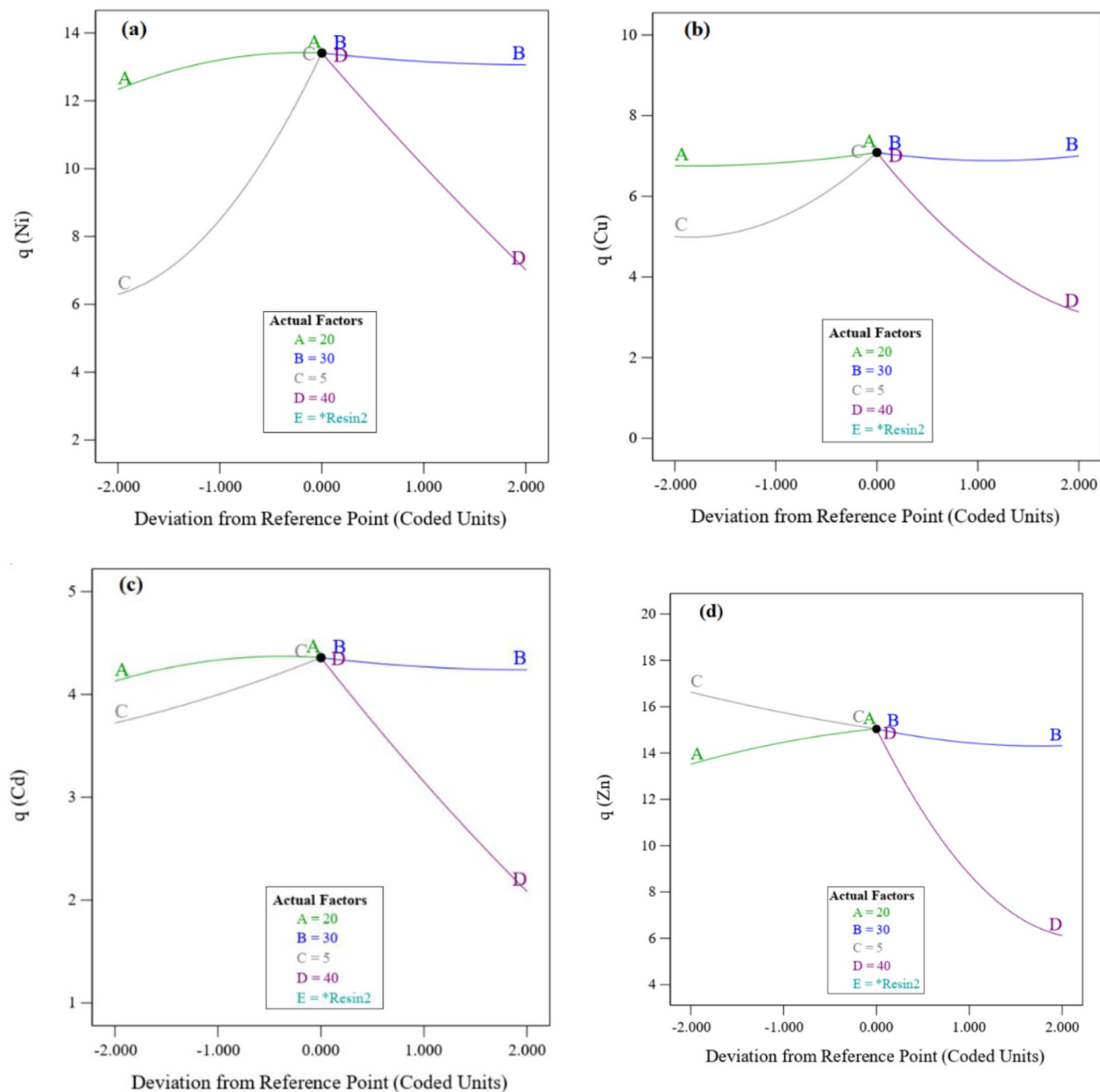


Figure 7. Effect of operating variables on (a) Ni, (b) Cu, (c) Cd and (d) Zn adsorption.

As the pH increases to 5, the negative charge of the resin surface increases and then adsorption rate increases⁸¹. But at pH > 5, both the mechanisms of surface adsorption and precipitation of the hydroxide phase have worked in parallel, which leads to an error increase in the dosage of adsorption. Therefore, the optimal pH is 5.

Adsorption kinetic

Knowing the adsorption kinetics is essential for the design of adsorption systems. As shown in Fig. 10, in the first stage, the adsorbate is located in the liquid layer around the adsorbent. In the second stage, due to the concentration difference between the surrounding liquid layer and the surface of the adsorbent, mass transfer occurs inside the cavities of the adsorbent. Finally, the adsorbates are adsorbed in the active sites inside the adsorbent.

The pseudo-first-order (PFO) kinetic model accomplished in cases where the initial concentration of the adsorbent is high, or there are few active sites in the adsorbent, or the adsorption is not controlled by the active sites of the adsorbent. Lagergren (1898) firstly proposed the PFO kinetic model by Eq. (12)⁶⁹.

$$q_t = q_e(1 - \exp(-k_1 t)) \quad (12)$$

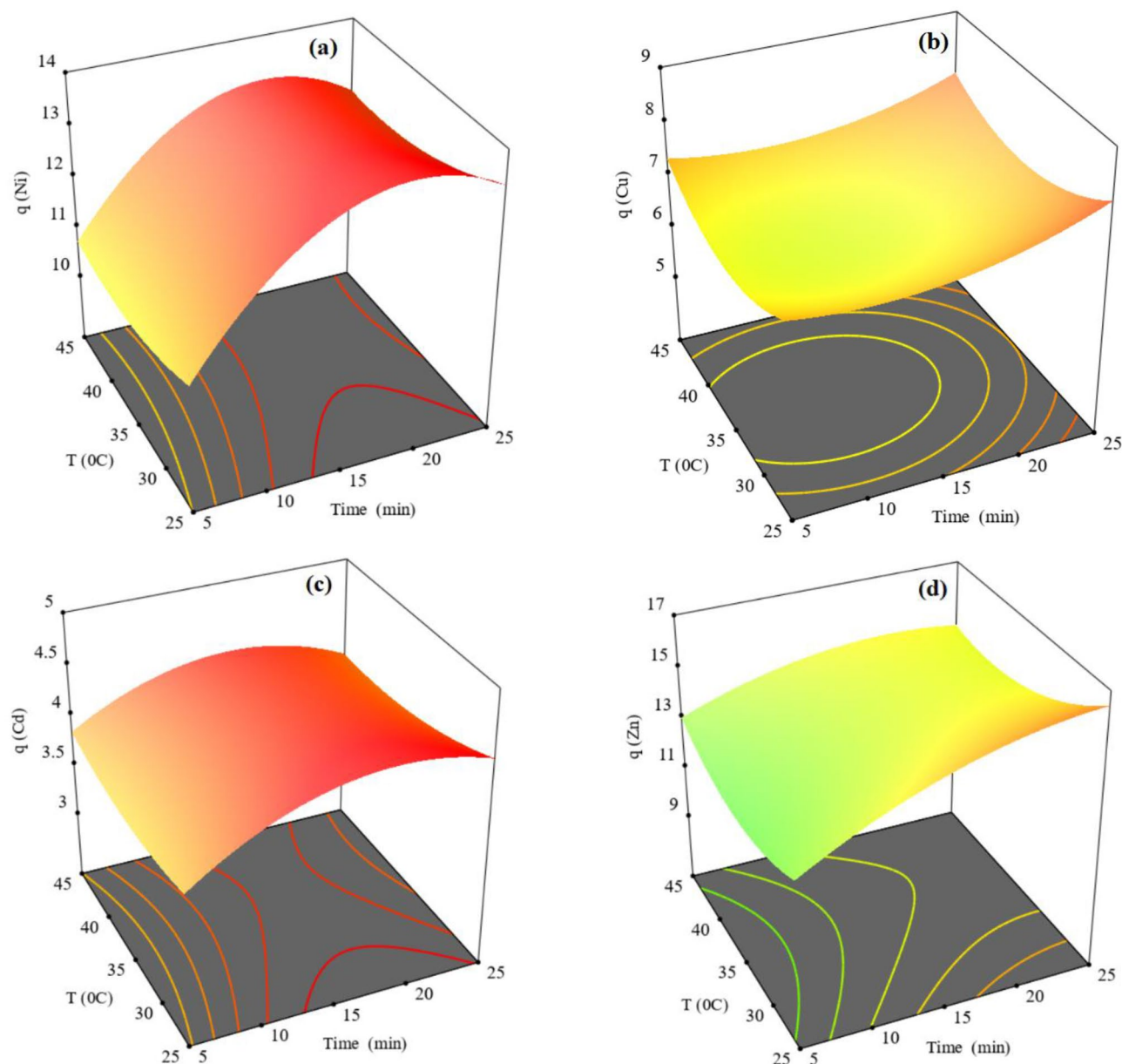


Figure 8. Response surfaces for (a) Ni, (b) Cu, (c) Cd and (d) Zn versus time and temperature.

The pseudo-second-order (PSO) kinetic model is used in conditions of low concentration of adsorbent and material adsorption in active sites of the adsorbent. Ho et al. (1996) firstly used the PSO kinetic model for adsorption of lead onto peat as Eq. (13)⁶⁹.

$$q_t = k_2 q_e^2 t / (1 + k_2 q_e t) \quad (13)$$

where q_e and q_t are the adsorption capacity per unit mass adsorbent (mg/g) at equilibrium and t time, respectively. The slope of the graph of q_e versus time indicates the speed constants (k_1 and k_2).

The adsorption kinetic experiments were carried out to evaluate the rate of nickel, copper, cadmium and zinc adsorption on the CH030. The plot of q_e versus time and R^2 values in both PFO and PSO kinetic models are presented in Fig. 11 and the parameters of the models are shown in Table 3. According to Table 4, R^2 values for the PSO model are higher than R^2 values for the PFO model. The experimental data fit better with the PSO model than the PFO model. The parameters in the PSO kinetics indicate that the rate-limiting step may be chemical adsorption related to the adsorption activity or the ion exchange between the adsorbent and the adsorbate. In physical adsorption, the bonding between adsorbate and adsorbent is by weak Van der Waals forces, but the chemical bond is formed between adsorbate and adsorbent surface⁷⁰ (Fig. 12).

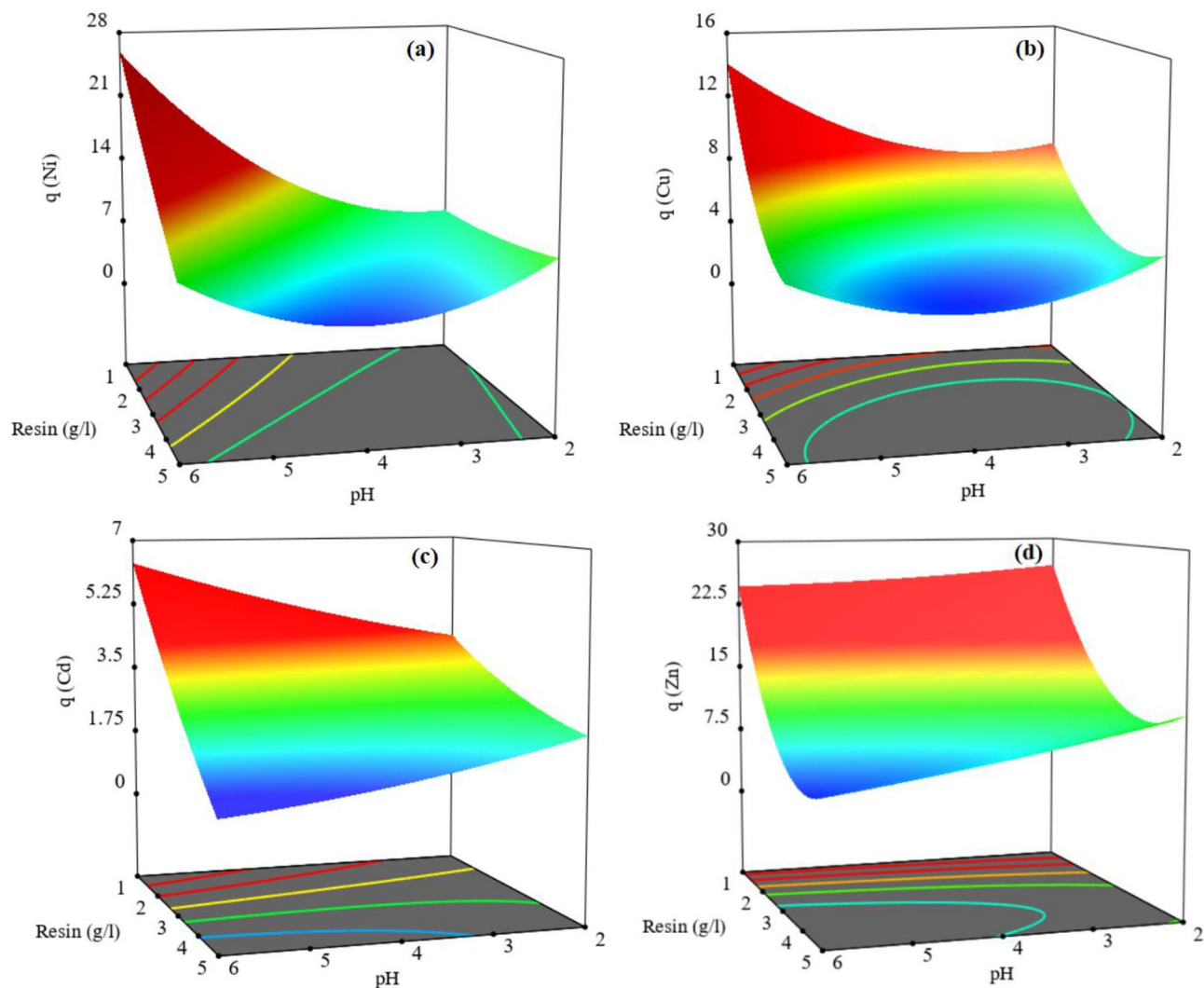


Figure 9. Response surfaces for (a) Ni, (b) Cu, (c) Cd and (d) Zn versus pH and resin dosage.

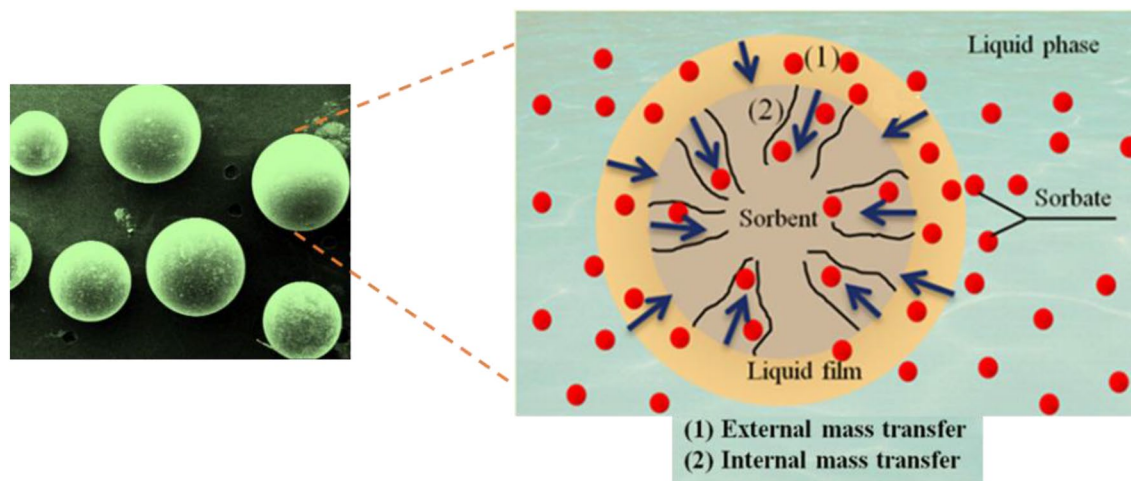


Figure 10. The interaction of functional groups of CH030 with metal cations.

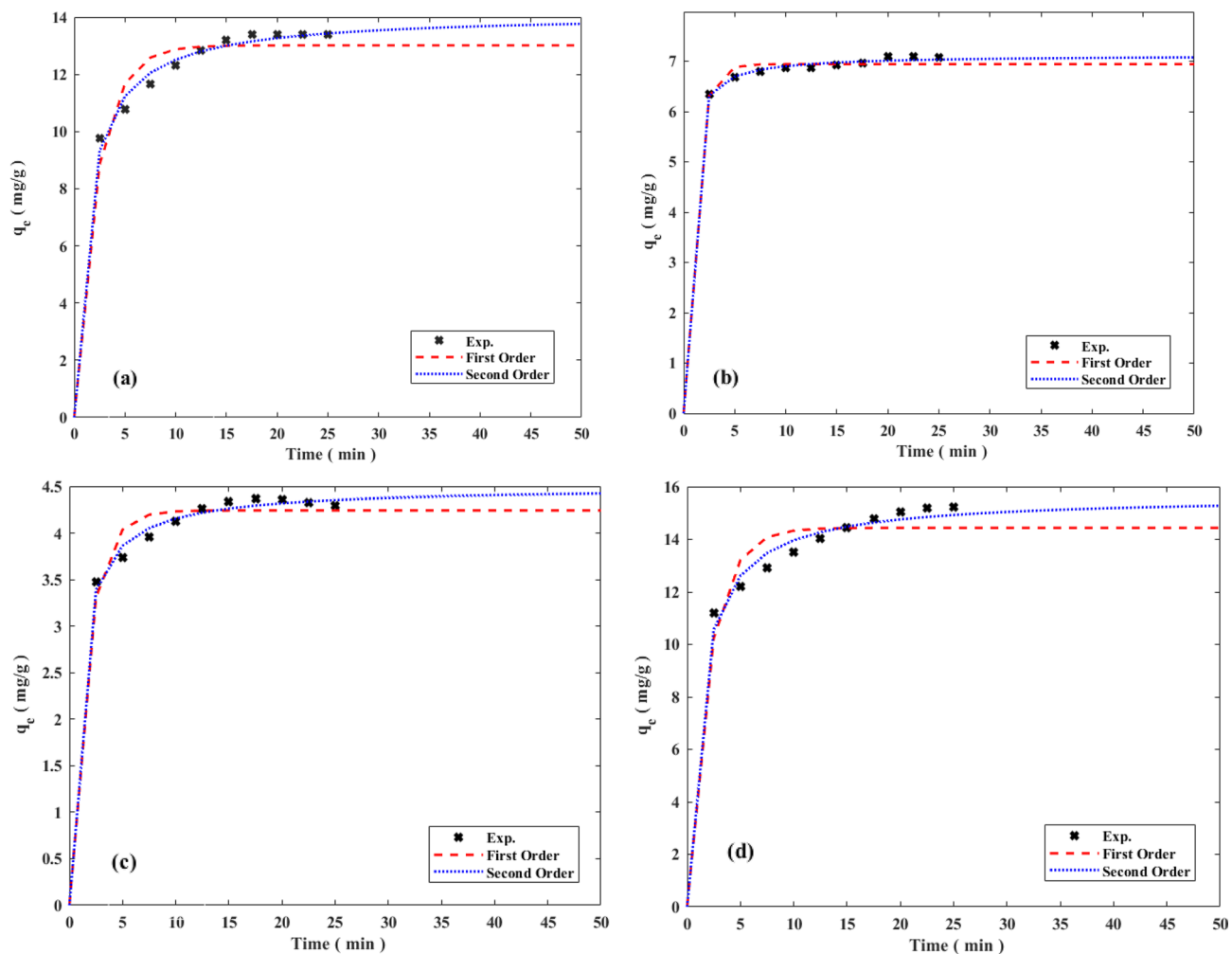


Figure 11. Adsorption kinetic plot for estimation of the parameters for (a) Ni, (b) Cu, (c) Cd and (d) Zn.

Kinetic models ions	PFO parameters			PSO parameters		
	q_c (mg/g)	Constant (k_1)	R^2	q_c (mg/g)	Constant (k_2)	R^2
Nickel	13.014	0.45522	0.88694	14.121	0.05507	0.97595
Copper	6.941	0.95985	0.84351	7.121	0.44174	0.97157
Cadmium	4.244	0.60581	0.85548	4.496	0.27237	0.96854
Zinc	14.440	0.49352	0.82300	15.650	0.05310	0.95618

Table 4. - Adsorption kinetic parameters of the Ni, Cu, Cd and Zn.

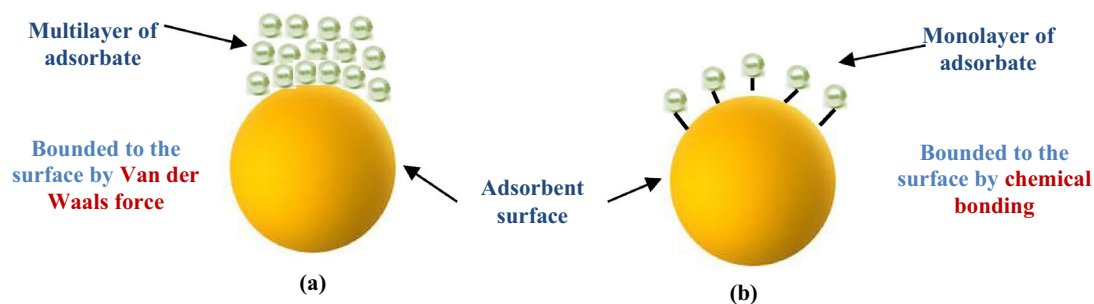


Figure 12. The mechanism of (a) physical and (b) chemical adsorption.

Adsorption thermodynamics

Thermodynamic parameters including free Gibbs energy (ΔG_0), enthalpy (ΔH_0), and entropy (ΔS_0) can be calculated using the following relations:

$$\Delta G = -RT \ln k_d \quad (14)$$

$$\Delta G = \Delta H - T \Delta S \quad (15)$$

$$\ln K_d = -\frac{\Delta H}{RT} + \frac{\Delta S}{R} \quad (16)$$

where R is calculated equal to $8.314 \text{ J mol}^{-1} \text{ K}^{-1}$. T is the solution absolute temperature (K) and K_d is distribution coefficient. The distribution coefficient is obtained from Eq. (17):

$$k_d = \frac{(C_0 - C_e)}{C_e} \times \frac{V}{W} \quad (17)$$

where C_0 and C_e are the initial and equilibrium concentrations in mg L^{-1} , V is the volume of the solution in ml and W is the mass of the adsorbent in $\text{g}^{71,72}$. For calculating the thermodynamic parameters, the effect of the temperature on the metals adsorption was investigated by time-based analyses, when the adsorption systems were analyzed until adsorbate concentration in the solution became constant (4 g/L).

Thermodynamic parameters for the adsorption were calculated from the variations of the thermodynamic equilibrium constant K_d that the van't Hoff equation is shown by drawing a linear graph of $\ln K_d$ versus $1/T$ at different temperatures based on Eq. (16) for these systems. It is possible to extract the values of adsorption enthalpy and adsorption entropy, respectively, using the slope and intercept of the plots in Fig. 13.

The ΔG values of the adsorbent CH030 at the different experimental temperatures were all negative, and the absolute values of ΔG increased with increasing of temperature (Table 5), which indicated that the adsorptions of nickel, copper, cadmium and zinc were beneficial with the increases of temperature. The ΔH values of CH030 adsorbent were greater than 0 (Table 4), indicating that the adsorption processes were endothermic, and adsorption rate increases with increasing temperature^{72,73}. The heat required for only ion exchange in the adsorption process is less than 8.4 kJ/mol^{74} but due to Table 5, ΔH values of four cations adsorption were much bigger than 8.4 kJ/mol that concluded in addition to ion exchange, chemical reaction also happened during the adsorption process. In general, the simultaneous adsorption of nickel, copper, cadmium and zinc on the CH030 resin is very complicated. The ΔS value for nickel, copper, cadmium and zinc was greater than 0 that indicates an increase in the free movement and degree of freedom of four cations in the solution^{71,75}. Size of the covalent radius of Zn is

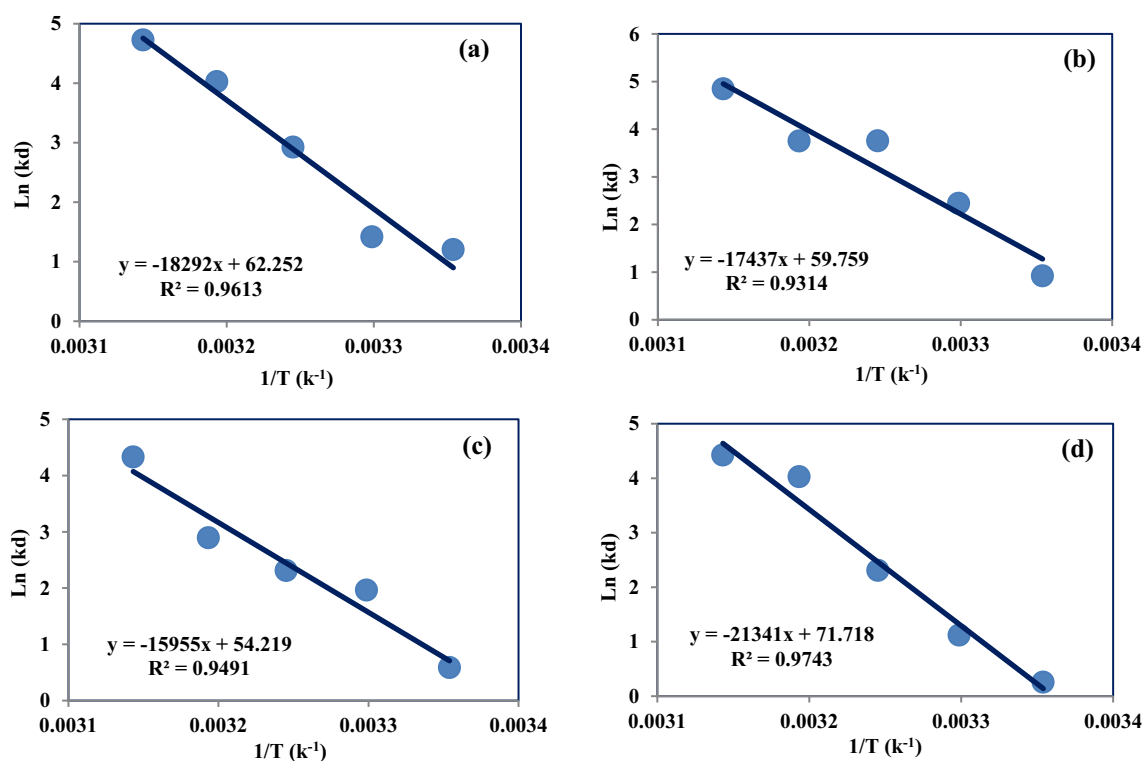


Figure 13. Van't Hoff Plot for estimation of the thermodynamic parameters for (a) Ni, (b) Cu, (c) Cd and (d) Zn.

T (°C)	K _d	ΔG (kJ/mol)	ΔS (J/mol K)	ΔH (kJ/mol)
Adsorption of nickel				
298.15	3.33	-2.23	0.52	152.09
303.15	4.12	-4.82		
308.15	18.62	-7.41		
313.15	55.95	-10.00		
318.15	112.86	-12.58		
Adsorption of copper				
298.15	2.52	-3.16	0.50	144.98
303.15	11.50	-5.65		
308.15	42.77	-8.13		
313.15	42.54	-10.61		
318.15	127.36	-13.10		
Adsorption of cadmium				
298.15	1.80	-1.75	0.45	132.66
303.15	7.11	-4.00		
308.15	10.08	-6.26		
313.15	18.05	-8.51		
318.15	75.86	-10.77		
Adsorption of zinc				
298.15	1.29	-0.35	0.60	177.44
303.15	3.06	-3.33		
308.15	10.04	-6.31		
313.15	56.01	-9.29		
318.15	83.46	-12.27		

Table 5. Thermodynamic parameters of the Ni, Cu, Cd and Zn adsorption on CH030 at different temperatures.

smaller than Ni, Cu and Cd, and it is possible to establish more bonds. As a result, irregularity or entropy of Zn increases and based on Eq. (15), enthalpy of Zn also increases more than other ions.

Conclusion

In this work, the optimization of simultaneous adsorption rate of Ni, Cu, Cd and Zn was done by predicting the model behaviour and realizing the effects of the operating parameters on adsorption with RSM. A suitable R² values through RSM-CCD of Ni, Cu, Cd and Zn are 0.9418, 0.9753, 0.9657 and 0.9189, respectively. Increasing the time of the adsorption to 20 min increases the adsorption rate because of the Ni, Cu, Cd and Zn ions have more chance to be adsorbed by active sites. Due to the weak bonds between the metal ions and the active sites of the resin at high temperatures, increasing the temperature does not have a significant effect on the adsorption rate. Increasing the resin dosage up to 2 g/L, which does not cause accumulation of particles, increases adsorption. At pH > 5, surface adsorption and precipitation of the hydroxide phase have happened, which leads to an error increase in the calculation of adsorption rate. The adsorption rate of two resins CH020 and CH030 was compared and more adsorption was done with resin CH030. The priority of metal adsorption in the optimal conditions is: Zn > Ni > Cu > Cd. In addition, Gibbs free energy values and high enthalpy values indicate the chemical interaction between the adsorbent surface and Ni, Cu, Cd and Zn ions in the solution. It is suggested to use the results of batch adsorption in a pilot-scale column in order to industrialize the process. Investigating the process conditions and economic issues is needed to transfer the laboratory results to the industrial scale. Also, comparing the results of this method with other methods can be considered.

Data availability

The data used and analyzed during the current study available from the corresponding author on reasonable request.

Received: 22 January 2024; Accepted: 28 March 2024

Published online: 29 March 2024

References

- Knska, D. K., Fila, D. & Hubicki, Z. Recovery of lanthanum(III) and nickel(II) ions from acidic solutions by the highly effective ion exchanger. *Molecules* **25**, 3718. <https://doi.org/10.3390/molecules25163718> (2020).
- Nosrati, A. *et al.* Agglomeration and column leaching behaviour of nickel laterite ores: Effect of ore mineralogy and particle size distribution. *Hydrometallurgy* **146**, 29–39. <https://doi.org/10.1016/j.hydromet.2014.03.004> (2014).
- International Agency for Research on Cancer (IARC), “and Dusts,” *Iarc Monogr.*, vol. 100, no. Arsenic, metals, fibres, and dusts, pp. 407–443, 2012, [Online]. <https://www.iarc.fr/>.

4. Sverdrup, H. U., Ragnarsdottir, K. V. & Koca, D. On modelling the global copper mining rates, market supply, copper price and the end of copper reserves. *Resour. Conserv. Recycl.* **87**, 158–174. <https://doi.org/10.1016/j.resconrec.2014.03.007> (2014).
5. Ghaemi, A., Torab-Mostaedi, M., Shahhosseini, S. & Asadollahzadeh, M. Characterization of Ag(I), Co(II) and Cu(II) removal process from aqueous solutions using dolomite powder. *Korean J. Chem. Eng.* **30**(1), 172–180. <https://doi.org/10.1007/s11814-012-0113-1> (2013).
6. L. Friberg, G. F. Nordberg, and V. B. Vouk, *Copper Handbook of the toxicology of metals*. Amsterdam, p. 57 (1981).
7. Masoumi, H., Ghaemi, A. & Ghanadzadeh Gilani, H. Experimental and RSM study of hypercrosslinked polystyrene in elimination of lead, cadmium and nickel ions in single and multi-component systems. *Chem. Eng. Res. Des.* **182**, 410–427. <https://doi.org/10.1016/j.cherd.2022.04.014> (2022).
8. Liu, Y. *et al.* Geogenic cadmium pollution and potential health risks, with emphasis on black shale. *J. Geochem. Explor.* **176**, 42–49. <https://doi.org/10.1016/j.jgexplo.2016.04.004> (2017).
9. Zhong, Q. *et al.* Cadmium isotopic fractionation in lead-zinc smelting process and signatures in fluvial sediments. *J. Hazard. Mater.* **411**(December 2020), 125015. <https://doi.org/10.1016/j.jhazmat.2020.125015> (2021).
10. Hussain, S. *et al.* Zinc essentiality, toxicity, and its bacterial bioremediation: A comprehensive insight. *Front. Microbiol.* **13**, 20. <https://doi.org/10.3389/fmicb.2022.900740> (2022).
11. M. J. Layton *et al.*, *Copper Book : 2021–2030 Outlook* (2021).
12. Kolbadinejad, S. & Ghaemi, A. Recovery and extraction of platinum from spent catalysts: A review. *Case Stud. Chem. Environ. Eng.* **7**(2), 100327. <https://doi.org/10.1016/j.csee.2023.100327> (2023).
13. Havlik, T. *Hydrometallurgy Principles and Applications*, A volume in Woodhead Publishing Series in Metals and Surface Engineering (2008).
14. Falagán, C., Grail, B. M. & Johnson, D. B. New approaches for extracting and recovering metals from mine tailings. *Miner. Eng.* **106**, 71–78. <https://doi.org/10.1016/j.mineng.2016.10.008> (2017).
15. Laatikainen, K., Lahtinen, M., Laatikainen, M. & Paatero, E. Copper removal by chelating adsorption in solution purification of hydrometallurgical zinc production. *Hydrometallurgy* **104**(1), 14–19. <https://doi.org/10.1016/j.hydromet.2010.04.005> (2010).
16. P. Aliprandini, M. Correa, A. Santanilla, J. Tenório, and D. C. R. Espinosa, Precipitation of metals from synthetic laterite nickel liquor by NaOH, in *8th Int. Semin. Process Hydrometall.* 28, pp. 1–8 (2016).
17. Moskalyk, R. R. & Alfantazi, A. M. Nickel laterite processing and electrowinning practice. *Miner. Eng.* **15**(8), 593–605. [https://doi.org/10.1016/S0892-6875\(02\)00083-3](https://doi.org/10.1016/S0892-6875(02)00083-3) (2002).
18. Bhaskara Sarma, P. V. R. & Reddy, B. R. Liquid-liquid extraction of nickel at macro-level concentration from sulphate/chloride solutions using phosphoric acid based extractants. *Miner. Eng.* **15**(6), 461–464. [https://doi.org/10.1016/S0892-6875\(02\)00063-8](https://doi.org/10.1016/S0892-6875(02)00063-8) (2002).
19. A. B. Botelho Junior, V. Rodrigues, D. C. R. Espinosa, and J. A. Tenório, Tailing Treatment of Nickel Mining, no. October, 2017.
20. Hale, D. K. Ion exchange technology. *Nature* **179**(4562), 723. <https://doi.org/10.1038/179723b0> (1957).
21. F. C. Nachod, Ion exchange theory and application, pp. 159–166, 255, 256, 1959.
22. Zargarollahi, H. New filamentary nano adsorber GZ-BAKI-TAC-Co-88 for rapid removal of cobalt ion from aqueous solutions using Beshel tire activated carbon. *J. Mar. Sci. Technol. Res.* **7**(2), 878 (2012).
23. Zainol, Z. & Nicol, M. J. Ion-exchange equilibria of Ni²⁺, Co²⁺, Mn²⁺ and Mg²⁺ with iminodiacetic acid chelating resin Amberlite IRC 748. *Hydrometallurgy* **99**(3–4), 175–180. <https://doi.org/10.1016/j.hydromet.2009.08.004> (2009).
24. Gando-Ferreira, L. M., Romão, I. S. & Quina, M. J. Equilibrium and kinetic studies on removal of Cu²⁺ and Cr³⁺ from aqueous solutions using a chelating resin. *Chem. Eng. J.* **172**(1), 277–286. <https://doi.org/10.1016/j.cej.2011.05.105> (2011).
25. Vakili, M. *et al.* Nickel ion removal from aqueous solutions through the adsorption process: A review. *Rev. Chem. Eng.* **37**(6), 755–778. <https://doi.org/10.1515/revce-2019-0047> (2021).
26. Stefan, D. S. & Meghea, I. Mechanism of simultaneous removal of Ca²⁺, Ni²⁺, Pb²⁺ and Al³⁺ ions from aqueous solutions using Purolite® S930 ion exchange resin. *Comptes Rendus Chim.* **17**(5), 496–502. <https://doi.org/10.1016/j.crci.2013.09.010> (2014).
27. Kuz'Min, V. I. & Kuz'Min, D. V. Sorption of nickel and copper from leach pulps of low-grade sulfide ores using Purolite S930 chelating resin. *Hydrometallurgy* **141**, 76–81. <https://doi.org/10.1016/j.hydromet.2013.10.007> (2014).
28. Littlejohn, P. & Vaughan, J. Selective elution of nickel and cobalt from iminodiacetic acid cation exchange resin using ammoniacal solutions. *Hydrometallurgy* **141**, 24–30. <https://doi.org/10.1016/j.hydromet.2013.10.009> (2014).
29. Li, B. *et al.* Efficient separation and high selectivity for nickel from cobalt-solution by a novel chelating resin: Batch, column and competition investigation. *Chem. Eng. J.* **195–196**, 31–39. <https://doi.org/10.1016/j.cej.2012.04.089> (2012).
30. O. Khelifi, M. Nacef, and A. M. Affoune, Nickel (II) adsorption from aqueous solutions by physico-chemically modified sewage sludge. *Iran. J. Chem. Chem. Eng. (IJCCCE)* **37**(1) - Serial Number 87 (2018). <https://doi.org/10.30492/IJCCCE.2018.29994>.
31. Shahriari, T., Karbassi, A. & Hirazinejad, M. Evaluation of nickel adsorption from plating wastewater by nanographite. *Environ. Sci.* **21**(2), 169–182. <https://doi.org/10.48308/envs.2023.1253> (2023).
32. Zhang, X. & Wang, X. Adsorption and desorption of Nickel(II) ions from aqueous solution by a lignocellulose/montmorillonite nanocomposite. *PLoS ONE* **10**(2), 1–21. <https://doi.org/10.1371/journal.pone.0117077> (2015).
33. Mendes, F. D. & Martins, A. H. Selective sorption of nickel and cobalt from sulphate solutions using chelating resins. *Int. J. Miner. Process.* **74**(1–4), 359–371. <https://doi.org/10.1016/j.minpro.2004.04.003> (2004).
34. S. Fathi, R. Rezaei Kalantari, A. Rashidi, and A. Karbasi, "Prototyping and determining the characteristics of a hybrid nano adsorbent made of graphene in order to absorb divalent nickel from aqueous solutions", no. 41 • pp. 161–171, 2019. <https://sid.ir/paper/169613/fa>.
35. Bleotu, I., Dorneanu, S.-A., Mureseanu, M., Gilca, E. & Ilea, P. Selective removal of Cu (II) from diluted aqueous media by an iminodiacetic acid functionalized resin. *Rev. Chim. -Bucharest-* **66**(6), 797–802 (2015).
36. Dragan, E. S., Dinu, M. V., Lisa, G. & Trochimczuk, A. W. Study on metal complexes of chelating resins bearing iminodiacetate groups. *Eur. Polym. J.* **45**(7), 2119–2130. <https://doi.org/10.1016/j.eurpolymj.2009.03.012> (2009).
37. Neto, I. F. F., Sousa, C. A., Brito, M. S. C. A., Futuro, A. M. & Soares, H. M. V. M. A simple and nearly-closed cycle process for recycling copper with high purity from end life printed circuit boards. *Sep. Purif. Technol.* **164**, 19–27. <https://doi.org/10.1016/j.seppur.2016.03.007> (2016).
38. Kolodyńska, D., Sofińska-Chmiel, W., Mendyk, E. & Hubicki, Z. DOWEX M 4195 and LEWATIT® MonoPlus TP 220 in heavy metal ions removal from acidic streams. *Sep. Sci. Technol.* **49**(13), 2003–2015. <https://doi.org/10.1080/01496395.2014.908920> (2014).
39. Wołowicz, A. & Hubicki, Z. The use of the chelating resin of a new generation Lewatit MonoPlus TP-220 with the bis-picolylamine functional groups in the removal of selected metal ions from acidic solutions. *Chem. Eng. J.* **197**, 493–508. <https://doi.org/10.1016/j.cej.2012.05.047> (2012).
40. Chen, C. Y., Chiang, C. L. & Chen, C. R. Removal of heavy metal ions by a chelating resin containing glycine as chelating groups. *Sep. Purif. Technol.* **54**(3), 396–403. <https://doi.org/10.1016/j.seppur.2006.10.020> (2007).
41. Lutfor, M. R. & Mashitah, M. Y. Synthesis of poly(hydroxamic acid)-poly(amidoxime) chelating ligands for removal of metals from industrial wastewater. *E-J. Chem.* **8**(3), 1038–1043. <https://doi.org/10.1155/2011/645628> (2011).
42. Zainol, Z. & Nicol, M. J. Comparative study of chelating ion exchange resins for the recovery of nickel and cobalt from laterite leach tailings. *Hydrometallurgy* **96**(4), 283–287. <https://doi.org/10.1016/j.hydromet.2008.11.005> (2009).
43. Edeballi, S. & Pehlivan, E. Evaluation of chelate and cation exchange resins to remove copper ions. *Powder Technol.* **301**, 520–525. <https://doi.org/10.1016/j.powtec.2016.06.011> (2016).

44. Monier, M., Ayad, D. M., Wei, Y. & Sarhan, A. A. Adsorption of Cu(II), Co(II), and Ni(II) ions by modified magnetic chitosan chelating resin. *J. Hazard. Mater.* **177**(1–3), 962–970. <https://doi.org/10.1016/j.jhazmat.2010.01.012> (2010).
45. Sulaiman, S. *et al.* Adsorptive removal of copper (II) ions from aqueous solution using a magnetite nano-adsorbent from mill scale waste: Synthesis, characterization, adsorption and kinetic modelling studies. *Nanoscale Res. Lett.* <https://doi.org/10.1186/s11671-021-03622-y> (2021).
46. Rani, P., Johar, R. & Jassal, P. S. Adsorption of nickel (II) ions from wastewater using glutaraldehyde cross-linked magnetic chitosan beads: Isotherm, kinetics and thermodynamics. *Water Sci. Technol.* **82**(10), 2193–2202. <https://doi.org/10.2166/wst.2020.459> (2020).
47. Kayalvizhi, K. *et al.* Adsorption of copper and nickel by using sawdust chitosan nanocomposite beads: A kinetic and thermodynamic study. *Environ. Res.* **203**(May 2021), 111814. <https://doi.org/10.1016/j.envres.2021.111814> (2022).
48. Zhao, X., Song, L., Zhang, Z., Wang, R. & Fu, J. Adsorption investigation of MA-DTPA chelating resin for Ni(II) and Cu(II) using experimental and DFT methods. *J. Mol. Struct.* **986**(1–3), 68–74. <https://doi.org/10.1016/j.molstruc.2010.11.049> (2011).
49. Onundi, Y. B., Mamun, A. A., Al Khatib, M. F. & Ahmed, Y. M. Adsorption of copper, nickel and lead ions from synthetic semiconductor industrial wastewater by palm shell activated carbon. *Int. J. Environ. Sci. Technol.* **7**(4), 751–758. <https://doi.org/10.1007/BF03326184> (2010).
50. Sočo, E. & Kalemkiewicz, J. Adsorption of nickel(II) and copper(II) ions from aqueous solution by coal fly ash. *J. Environ. Chem. Eng.* **1**(3), 581–588. <https://doi.org/10.1016/j.jece.2013.06.029> (2013).
51. Zeng, G. *et al.* Adsorption of heavy metal ions copper, cadmium and nickel by *Microcystis aeruginosa*. *Int. J. Environ. Res. Public Health* <https://doi.org/10.3390/ijerph192113867> (2022).
52. Alatabe, M. J. Adsorption of copper (II) ions from aqueous solution onto activated carbon prepared from cane papyrus. *Pollution* **4**(4), 649–662. <https://doi.org/10.22059/poll.2018.249931.377> (2018).
53. Baykara, H., Solorzano, M. D. L. M., Echeverria, J. J. D., Cornejo, M. H. & Tapia-Bastidas, C. V. The use of zeolite-based geopolymers as adsorbent for copper removal from aqueous media. *R. Soc. Open Sci.* <https://doi.org/10.1098/rsos.211644> (2022).
54. Danesh, N., Ghorbani, M. & Marjani, A. Separation of copper ions by nanocomposites using adsorption process. *Sci. Rep.* **11**(1), 1–23. <https://doi.org/10.1038/s41598-020-80914-w> (2021).
55. Perez, I. D., Anes, I. A., Botelho Junior, A. B. & Espinosa, D. C. R. Comparative study of selective copper recovery techniques from nickel laterite leach waste towards a competitive sustainable extractive process. *Clean. Eng. Technol.* **1**(December), 100031. <https://doi.org/10.1016/j.clet.2020.100031> (2020).
56. A. B. Botelho Junior, M. M. Jimenez Correa, C. Rosario, D. C. R. Espinosa, and J. A. S. Tenório, Recovery of metals from nickel laterite leach waste using chelating resin, in *10th Int. Semin. Process Hydrometall.*, no. August, pp. 1–8, 2018.
57. Wołowicz, A. & Hubicki, Z. Enhanced removal of copper(II) from acidic streams using functional resins: Batch and column studies. *J. Mater. Sci.* **55**(28), 13687–13715. <https://doi.org/10.1007/s10853-020-04982-z> (2020).
58. Wołowicz, A., Staszak, K. & Hubicki, Z. Removal of copper(II) in the presence of sodium dodecylbenzene sulfonate from acidic effluents using adsorption on ion exchangers and micellar-enhanced ultrafiltration methods. *Molecules* <https://doi.org/10.3390/molecules27082430> (2022).
59. W.L.F. Armarego, Purification of Laboratory Chemicals (Ninth edition) Part 2: Inorganic Chemicals, Catalysts, Biochemicals, Physiologically Active Chemicals, Nanomaterials 2022, 586–630. <https://doi.org/10.1016/B978-0-323-90968-6.50005-9>.
60. Marin, N. M. *et al.* Preparation of eco-friendly chelating resins and their applications for water treatment. *Polymers (Basel)* <https://doi.org/10.3390/polym15102251> (2023).
61. N. M. Marin, A. Ficaí, L. A. Constantin, L. Motelica, and R. Trusca, “Cu²⁺ and Pb²⁺ Removal,” 2022.
62. Srivastava, A. *et al.* Response surface methodology and artificial neural network modelling for the performance evaluation of pilot-scale hybrid nanofiltration (NF) & reverse osmosis (RO) membrane system for the treatment of brackish ground water. *J. Environ. Manag.* **278**(P1), 111497. <https://doi.org/10.1016/j.jenvman.2020.111497> (2021).
63. Patidar, R. & Srivastava, V. C. Mechanistic insight into ultrasound-induced enhancement of electrochemical oxidation of ofloxacin: Multi-response optimization and cost analysis. *Chemosphere* **257**, 127121. <https://doi.org/10.1016/j.chemosphere.2020.127121> (2020).
64. Kumar, J., Joshi, H. & Malyan, S. K. Removal of copper, nickel, and zinc ions from an aqueous solution through electrochemical and nanofiltration membrane processes. *Appl. Sci.* <https://doi.org/10.3390/app12010280> (2022).
65. Ghaemi, A., Torab-Mostaedi, M. & Ghannadi-Maragheh, M. Characterizations of strontium(II) and barium(II) adsorption from aqueous solutions using dolomite powder. *J. Hazard. Mater.* **190**(1–3), 916–921. <https://doi.org/10.1016/j.jhazmat.2011.04.006> (2011).
66. S. G. Santiago Urréjola-Madrinán, Iñaki Paz-Armeda, “Application of Central Composite Design for Optimization of Adsorption of Chromium(VI),” no. Vi, 2022.
67. N. Ivanova, V. Gugleva, M. Dobрева, I. Pehlivanov, S. Stefanov, and V. Andonova, “We are IntechOpen, the world’s leading publisher of Open Access books Built by scientists , for scientists TOP 1%,” *Intech*, vol. i, no. tourism, p. 13, 2016.
68. Khoshraftar, Z. & Ghaemi, A. Prediction of CO₂ solubility in water at high pressure and temperature via deep learning and response surface methodology. *Case Stud. Chem. Environ. Eng.* <https://doi.org/10.1016/j.cscee.2023.100338> (2023).
69. Wang, J. & Guo, X. Adsorption kinetic models: Physical meanings, applications, and solving methods. *J. Hazard. Mater.* **390**(November 2019), 122156. <https://doi.org/10.1016/j.jhazmat.2020.122156> (2020).
70. Rudi, N. N. *et al.* Evolution of adsorption process for manganese removal in water via agricultural waste adsorbents. *Heliyon* **6**(9), e05049. <https://doi.org/10.1016/j.heliyon.2020.e05049> (2020).
71. Guo, X. *et al.* Adsorption mechanism of hexavalent chromium on biochar: Kinetic, thermodynamic, and characterization studies. *ACS Omega* **5**(42), 27323–27331. <https://doi.org/10.1021/acsomega.0c03652> (2020).
72. Lyubchik, S. I. *et al.* Kinetics and thermodynamics of the Cr(III) adsorption on the activated carbon from co-mingled wastes. *Colloids Surf. A Physicochem. Eng. Asp.* **242**(1–3), 151–158. <https://doi.org/10.1016/j.colsurfa.2004.04.066> (2004).
73. Rahmati, A., Ghaemi, A. & Samadfam, M. Kinetic and thermodynamic studies of uranium(VI) adsorption using Amberlite IRA-910 resin. *Ann. Nucl. Energy* **39**(1), 42–48. <https://doi.org/10.1016/j.anucene.2011.09.006> (2012).
74. Tran, H. N., You, S. J., Hosseini-Bandegharai, A. & Chao, H. P. Mistakes and inconsistencies regarding adsorption of contaminants from aqueous solutions: A critical review. *Water Res.* **120**, 88–116. <https://doi.org/10.1016/j.watres.2017.04.014> (2017).
75. Mohammadi, M., Ghaemi, A., Torab-Mostaedi, M., Asadollahzadeh, M. & Hemmati, A. Adsorption of cadmium (II) and nickel (II) on dolomite powder. *Desalin. Water Treat.* **53**(1), 149–157. <https://doi.org/10.1080/19443994.2013.836990> (2015).
76. Malamis, S. & Katsou, E. A review on zinc and nickel adsorption on natural and modified zeolite, bentonite and vermiculite: Examination of process parameters, kinetics and isotherms. *J. Hazard. Mater.* **252–253**, 428–461. <https://doi.org/10.1016/j.jhazmat.2013.03.024> (2013).
77. Pahlavanzadeh, H. & Motamedi, M. Adsorption of nickel, ni(ii), in aqueous solution by modified zeolite as a cation-exchange adsorbent. *J. Chem. Eng. Data* **65**(1), 185–197. <https://doi.org/10.1021/acs.jced.9b00868> (2020).
78. Mahmoud, R. K., Mohamed, F., Gaber, E. & Abdel-Gawad, O. F. Insights into the synergistic removal of Copper(II), Cadmium(II), and Chromium(III) ions using modified chitosan based on Schiff bases-g-poly(acrylonitrile). *ACS Omega* **7**(46), 42012–42026. <https://doi.org/10.1021/acsomega.2c03809> (2022).

79. Muntean, S. G., Halip, L., Nistor, M. A. & Păcurariu, C. Removal of metal ions via adsorption using carbon magnetic nanocomposites: optimization through response surface methodology, kinetic and thermodynamic studies. *Magnetochemistry* **9**(7), 25. <https://doi.org/10.3390/magnetochemistry9070163> (2023).
80. El-Sadaawy, M. & Abdelwahab, O. Adsorptive removal of nickel from aqueous solutions by activated carbons from doum seed (*Hyphaenethebaica*) coat. *Alex. Eng. J.* **53**(2), 399–408. <https://doi.org/10.1016/j.aej.2014.03.014> (2014).
81. Ossman, M. E. & Abdelfattah, M. Response surface methodology for optimising the operating conditions of nickel(II) adsorption. *J. Environ. Eng. Sci.* **10**(2), 27–33. <https://doi.org/10.1680/jees.14.00011> (2015).
82. Aregawi, B. H. & Mengistie, A. A. Removal of Ni(II) from aqueous solution using leaf, bark and seed of moringa stenopetala adsorbents. *Bull. Chem. Soc. Ethiop.* **27**(1), 35–47. <https://doi.org/10.4314/bcse.v27i1.4> (2013).
83. Rao, M. D., Singh, K. K., Morrison, C. A. & Love, J. B. Optimization of process parameters for the selective leaching of copper, nickel and isolation of gold from obsolete mobile phone PCBs. *Clean. Eng. Technol.* **4**, 100180. <https://doi.org/10.1016/j.clet.2021.100180> (2021).
84. Pan, S. Y., Syu, W. J., Chang, T. K. & Lee, C. H. A multiple model approach for evaluating the performance of time-lapse capsules in trapping heavy metals from water bodies. *RSC Adv.* **10**(28), 16490–16501. <https://doi.org/10.1039/d0ra03017a> (2020).
85. Bao, S., Chen, Q., Zhang, Y. & Tian, X. Optimization of preparation conditions of composite electrodes for selective adsorption of vanadium in CDI by response surface methodology. *Chem. Eng. Res. Des.* **168**, 37–45. <https://doi.org/10.1016/j.cherd.2021.01.032> (2021).
86. Ajiboye, A. E., Olashinde, F. E., Adebayo, O. A. & Ajayi, O. J. Recovery of copper and nickel from polymetallic sulphate leach solution of printed circuit boards using Dowex M 4195. *Physicochem. Probl. Miner. Process.* **55**(5), 1156–1164. <https://doi.org/10.5277/ppmp19038> (2019).

Author contributions

S.K.: Conceptualization, Methodology, Software, Conceived and designed the experiments, Validation, Formal analysis, Investigation, Resources, Data curation, Writing - original draft, Writing - review & editing, Supervision Visualization, Project administration. A.G.: Conceptualization, Methodology, Software, Conceived and designed the experiments, Validation, Formal analysis, Investigation, Resources, Data curation, Writing - original draft, Writing - review & editing, Supervision Visualization, Project administration. Supervision, Funding acquisition, Software, Validation, Formal analysis, Investigation, Resources, Visualization.

Competing interests

The authors declare no competing interests.

Additional information

Correspondence and requests for materials should be addressed to A.G.

Reprints and permissions information is available at www.nature.com/reprints.

Publisher's note Springer Nature remains neutral with regard to jurisdictional claims in published maps and institutional affiliations.



Open Access This article is licensed under a Creative Commons Attribution 4.0 International License, which permits use, sharing, adaptation, distribution and reproduction in any medium or format, as long as you give appropriate credit to the original author(s) and the source, provide a link to the Creative Commons licence, and indicate if changes were made. The images or other third party material in this article are included in the article's Creative Commons licence, unless indicated otherwise in a credit line to the material. If material is not included in the article's Creative Commons licence and your intended use is not permitted by statutory regulation or exceeds the permitted use, you will need to obtain permission directly from the copyright holder. To view a copy of this licence, visit <http://creativecommons.org/licenses/by/4.0/>.

© The Author(s) 2024